Combined Effect of Irradiation and Temperature on the Mechanical Strength of Inconel 800H and AISI 310 Alloys for In-Core Components of a Gen-IV SCWR

Robert J. Klassen[1]
Department of Mechanical and Materials Engineering,
University of Western Ontario,
1151 Richmond Street,
London, ON N6A 3K7, Canada
e-mail: rjklasse@uwo.ca

Heygaan Rajakumar
Department of Mechanical and Materials Engineering,
University of Western Ontario,
1151 Richmond Street,
London, ON N6A 3K7, Canada
e-mail: hrajakum@uwo.ca

Inconel 800H and AISI 310 alloy samples were exposed to Fe^{4+} *ions to simulate neutron irradiation damage, and then annealed at 400°C and 500°C to study the kinetics of thermal recovery of the irradiation damage. The increase in hardness with ion irradiation and the decrease in hardness due to thermal recovery were recorded. Our findings suggest that under thermal and neutron irradiation conditions envisaged for the Canadian Gen-IV SCWR concept, both alloys will experience significant irradiation hardening; however, this will be concurrently negated by even more rapid thermal recovery of the irradiation damage.* [DOI: 10.1115/1.4031015]

1 Introduction

A primary challenge associated with the proposed Canadian Gen-IV SCWR concept is the selection of suitable alloys for the nuclear fuel cladding and pressure tube liner components [1,2]. The alloys must be capable of enduring high levels of neutron irradiation in supercritical water at temperature up to about 750°C. Two alloys currently being studied for this application are AISI 310 and Inconel 800H. To date, little is known of the effect of prolonged, high-temperature neutron irradiation on the mechanical properties of these materials.

It is well known that neutron irradiation has a significant hardening effect on crystalline material as a result of the generation of neutron-induced crystal defects in the material [3]. The effect of neutron irradiation on the hardening of common nuclear materials, such as iron- and zirconium-based alloys, is now quite well characterized over the 250–350°C temperature range typical of current water-cooled reactors. The rate of neutron irradiation hardening above this temperature will, presumably, be affected by faster rates of thermal recovery of the irradiation damage; however, this has yet to be quantified experimentally.

Studies of the effect of neutron irradiation hardening have traditionally been done by direct in-reactor exposure of test samples followed by mechanical testing in radiation-shielded facilities. These tests are very time-consuming and expensive. Recently, there is increased use of high-energy ($E > 1$ MeV), self-similar ion irradiation to invoke irradiation hardening at a rate that is orders of magnitude faster than in-reactor neutron irradiation [4–8]. The depth of penetration of high-energy heavy ions into crystalline solids is only several micrometers; therefore, the use of ion irradiation to simulate neutron irradiation hardening must be accompanied with a nano-mechanical testing technique capable of sampling the hardness of this small region.

This paper reports some results from our study of the effect of high-energy Fe^{4+} irradiation on the hardness of the AISI 310 and Inconel 800H alloys under temperature conditions of 400°C and 500°C. We approach this problem by (1) measuring the rate of increase in hardness as a function of ion irradiation damage, and then (2) measuring the rate of decrease of hardness due to thermal recovery of the ion-induced damage. To this end, we perform room-temperature indentation hardness tests on both alloys exposed to various levels of Fe^{4+} irradiation and then expose these samples to isothermal heating, at 400°C and 500°C, for various lengths of time to measure the rate of recovery of the indentation hardness. This research is part of a larger study to assess the suitability of these alloys for use as high-temperature fuel cladding and pressure tube liner material in the proposed Canadian Gen-IV SCWR.

2 Procedure

2.1 Test Material. The chemical compositions of the AISI 310 and Inconel 800H alloys are given in Table 1. Polished surfaces, 12.7×12.7 mm, were prepared from each material by conventional mechanical grinding and polishing techniques. The final polishing step was performed with an aqueous suspension of 0.05 μm Al_2O_3 abrasive particles. The polished samples were then annealed for 20 min in a protective atmosphere at 1000°C to remove residual cold-work from the grinding/polishing steps. The annealed samples were then lightly polished with the 0.05 μm Al_2O_3 suspension to remove any surface oxidation resulting from annealing. The etched microstructure of the alloys is shown in Fig. 1 and consists of large equiaxed grains of 50–100 μm diameter.

2.2 Ion Irradiation. The polished unetched samples were irradiated with 8.0 MeV Fe^{4+} ions at the Tandetron Ion Accelerator facility at the University of Western Ontario. The samples were masked such that different regions of the polished surface received different levels of ion dosage. The SRIM software (http://www.srim.org/) was used to calculate the ion penetration depth (Fig. 2) and the required ion dosage necessary to invoke specific levels of irradiation damage. The level of irradiation damage is expressed in units of displacements per atom (dpa) and was calculated from the number of ion-induced atom displacements as determined by SRIM using the Kinchin–Pease model. Regions of the AISI 310 samples

[1]Corresponding author.

Manuscript received May 7, 2015; final manuscript received June 24, 2015; published online February 29, 2016. Assoc. Editor: Thomas Schulenberg.

Table 1 Chemical composition, in weight percent, of the two alloys used in this study

	C	Al	Si	P	S	Ti	Cr	Mn	Fe	Ni	Cu	Mo
AISI 310	0.08	–	0.75	0.05	0.03	–	25.00	2.00	50.35	20.50	0.50	0.75
Inconel 800H	0.08	1.40	1.00	0.05	0.02	1.40	21.00	1.50	39.50	33.00	0.75	–

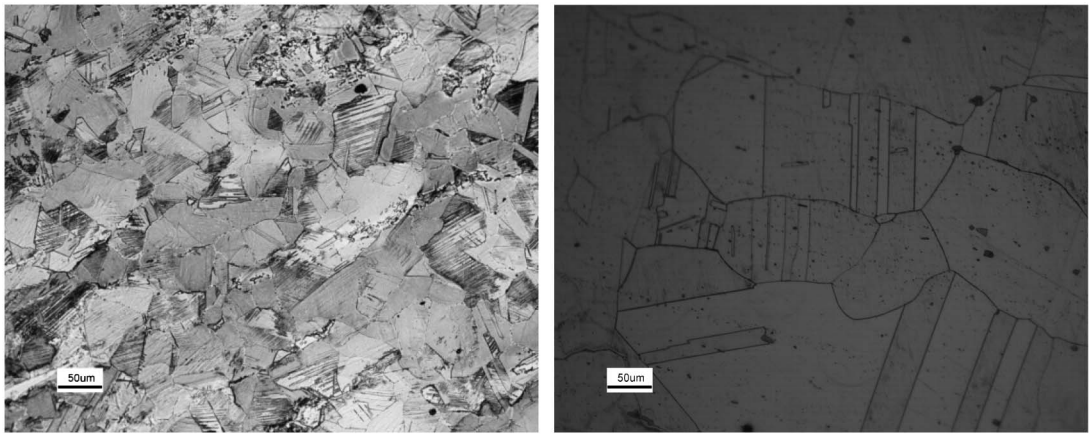

Fig. 1 Micrographs of the etched surfaces of (*a*) AISI 310 and (*b*) Inconel 800H

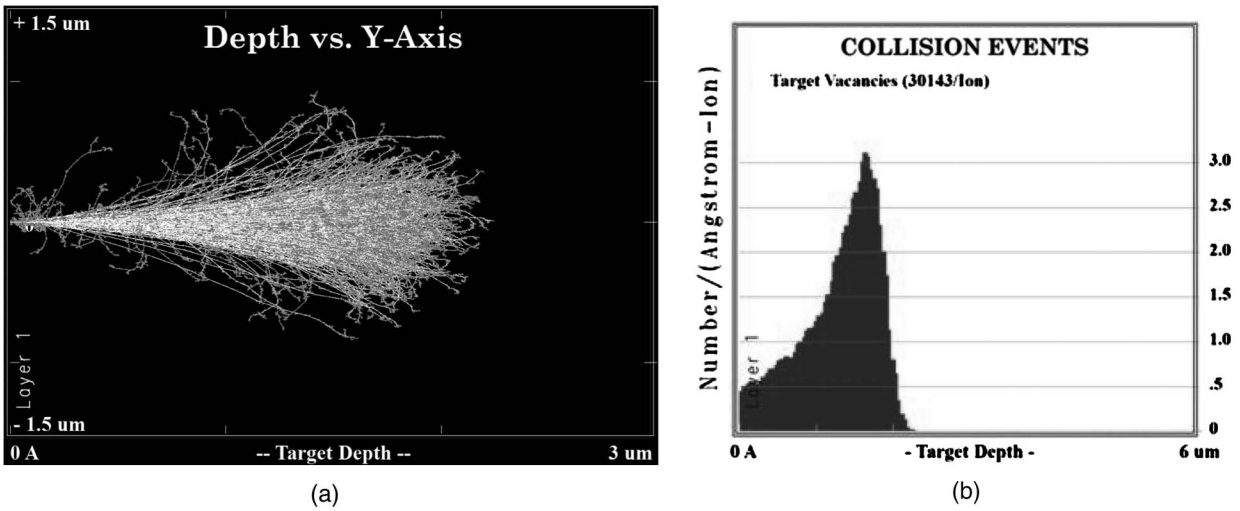

Fig. 2 SRIM simulation of the penetration of 8.0 MeV Fe^{4+} ions into the AISI 310 alloy: (*a*) The simulated ion trajectories. (*b*) The calculated number of ion/atom collisions per Angstrom travelled by the ion as a function of penetration depth. The maximum ion irradiation damage occurs at a depth between 1 and 2 μm.

were exposed to ion dosage levels corresponding to 0.01–10 dpa, whereas regions of the Inconel 800H samples were irradiated to levels from 0.10 to 15 dpa (Table 2).

2.3 Indentation Hardness Tests. Multiple indentation hardness tests were performed on each dpa region of the ion-irradiated samples. The tests were performed with a diamond Berkovich indenter at a constant ratio of indentation loading rate/load, $\dot{F}/F = 0.05\ s^{-1}$. Multiple partial unloadings were performed during each indentation test to allow determination of the indentation hardness at various indentation depths. The plastic indentation depth h was calculated using the Doerner–Nix equation [9]. The indentation hardness H was calculated as

$$H = \frac{F}{A(h)} \tag{1}$$

where $A(h)$ is a high-order polynomial shape function describing the dependence of the projected indentation contact area A upon the indentation depth h. The function $A(h)$ was determined from calibration tests performed by indentation of fused silica.

The indented ion-irradiated samples were then annealed at 400°C and 500°C for various lengths of time from 1 to 100 min (Table 2). The annealing was performed in an electrical resistance tube furnace containing an argon atmosphere. The samples were removed from the furnace after each annealing time, and multiple indentation hardness measurements were performed using the

Table 2 Conditions of irradiation damage (dpa), annealing temperature, and annealing time at which indentation hardness tests were performed on the AISI 310 (•) and Inconel 800H (■) samples

Irradiation damage (dpa)	As-irradiated	400°C anneal (minutes)				500°C anneal (minutes)			
		1	2	10	100	1	10	50	100
0	•, ■	•, ■	•, ■	•, ■	•, ■	•, ■	•, ■	•, ■	•, ■
0.01	•, ■					•, ■	•, ■	•, ■	•, ■
0.1	•, ■	•	•	•	•	•, ■	•, ■	•, ■	•, ■
0.5	•	•	•	•	•				
1	•, ■	•	•	•	•	•, ■	•, ■	•, ■	•, ■
2	•	•	•	•	•				
4	•	•	•	•	•				
8	•	•	•	•	•				
10	•, ■					•, ■	•, ■	•, ■	•, ■
15	■	■	■	■	■				

method described earlier. Typically, 10 indentations, each containing nine partial unloading, were performed at each of the 86 test conditions shown in Table 2.

3 Results and Discussion

3.1 Effect of Ion Irradiation on the Indentation Hardness. Figure 3 shows indentation force versus depth curves for the AISI 310 alloy in the nonirradiated and the ion-irradiated (8 dpa) conditions. The material clearly becomes hardened as a result of ion irradiation. The hardness of both the AISI 310 and Inconel 800H alloys displayed an indentation depth effect with higher hardness, when the indentation depth was small (Fig. 4). This is consistent with the well-known indentation-depth dependence of hardness that is generally observed for ductile materials and reflects the increased "geometrically necessary" dislocation density in the plastic zone around the shallow indentations of depth less than about 1 μm [10].

Although the ion-irradiated material displayed higher hardness than the nonirradiated material at all indentation depths, the increase in hardness was greater for indentations of depth less than about 500 nm (Fig. 4). This is likely due to the geometry of the test system as shown in Fig. 5. As the hardness reflects the average stress necessary to invoke plastic strain in a finite volume beneath the indenter, only indentations of depths less than that in which the plastic zone does not extend significantly beyond the ion penetration depth will reflect the true effect of irradiation damage on the hardness.

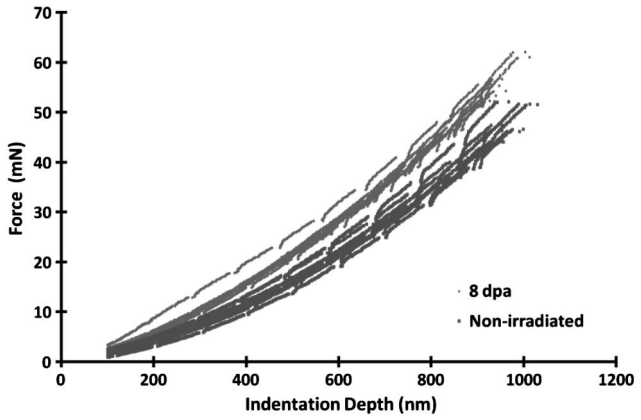

Fig. 3 Indentation force versus depth from multiple tests performed on the AISI 310 alloy in the nonirradiated and the ion-irradiated (8 dpa) conditions. The data from the partial unloading were removed from this graph to display more clearly the force–depth trend.

Johnson proposed the following equation for the radius c of a hemispherical plastic zone beneath a conical indenter of flank angle β and width a (Fig. 5)

$$\frac{c}{a} = \left[\frac{E^* \tan\beta}{6\sigma_y(1-\nu)} + \frac{2}{3}\left(\frac{1-2\nu}{1-\nu}\right)\right]^{\frac{1}{3}} \tag{2}$$

where σ_y is the flow stress; v is the Poisson's ratio of the indented material; and E^* is the reduced elastic modulus of the indenter/substrate system [11]. The values representative of our test material and indenter are substituted in Eq. (2): $\beta = 20°$, $v = 0.36$, $E^* = 184$ GPa, and $s_{y(\text{irradiated})} \approx H_{\text{irradiated}}/3$ [12], where $H_{\text{irrad.}} \approx 4.0$ GPa. We find that the radius c of the plastic zone is about 1.15, 2.31, and 4.61 μm for indentation depths h of 100, 200, and 400 nm, respectively. This relation, $c = 11.5h$, is very close to $c = 12h$ calculated using elastic–plastic finite element analyses for pyramidal indentations of the same geometry as that used in this study [13,14]. As the calculated depth of the ion-irradiation hardening in our study is slightly more than 2 μm, and based upon the analysis earlier, we will assess the effect of ion irradiation on the hardness by considering the hardness data from indentation depths of 200 and 400 nm.

The average nonirradiated indentation hardness at depths of 200 and 400 nm was 3.6 and 3.1 GPa for the AISI 310 and 4.1 and 3.7 GPa for the Inconel 800H alloys. Figure 6 shows the effect of increasing Fe^{4+} ion irradiation damage, in units of dpa, on the average hardness of both alloys. The average indentation hardness was determined from multiple, typically 10, indentations at each indentation depth, 200 and 400 nm, and each dpa level. The scatter in the data in Fig. 6 indicates the variability in the hardness arising primarily as a result of surface roughness.

The following power-law functions for hardness H, in units of GPa, were obtained by fitting to the data in Fig. 6(*a*) for the 200 nm indentations

$$H_{200\,\text{nm AISI 310}} = 3.6 + 1.6(\text{dpa})^{0.09} \tag{3}$$

$$H_{200\,\text{nm Inconel 800H}} = 4.1 + 2.5(\text{dpa})^{0.02} \tag{4}$$

One can see that the two alloys show very similar irradiation-hardening characteristics, with rapidly increasing hardness after small amounts of irradiation damage such that H increases by 20–40% after about 1.0 dpa of irradiation damage. These hardness values, and the extent of irradiation hardening at low dpa levels, are very consistent with previously reported findings for the ion-irradiated AISI 316 alloy [15].

3.2 Effect of Annealing on Recovery of Ion-Irradiation Hardening. Figure 7 indicates how the average room-temperature indentation hardness H, for 200 nm deep indentations, decreases

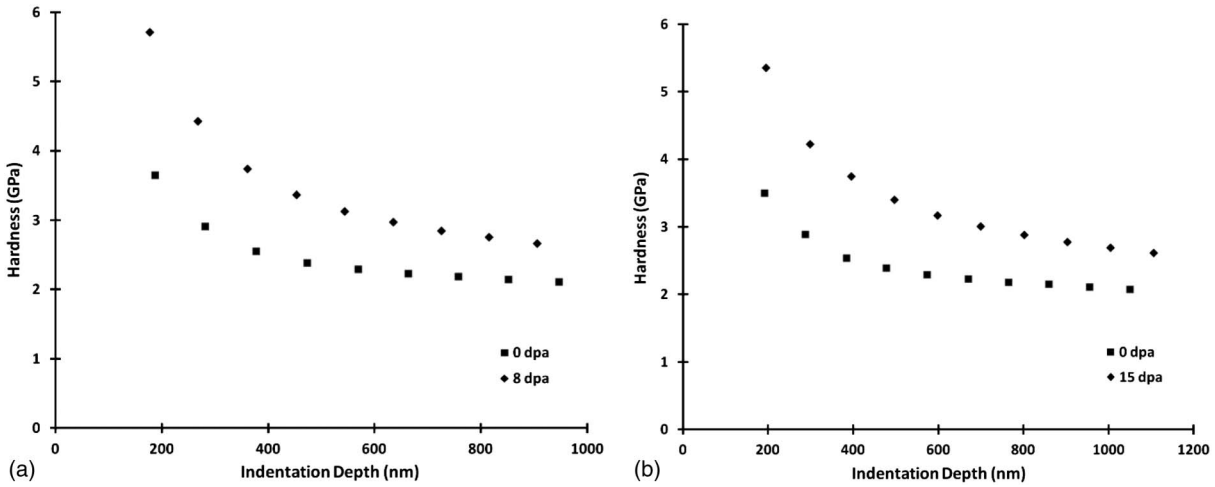

Fig. 4 Indentation hardness versus depth for (*a*) the AISI 310 alloy in the nonirradiated and the ion-irradiated (8 dpa) conditions and (*b*) the Inconel 800H alloy in the nonirradiated and the ion-irradiated (15 dpa) conditions. Each series of data was obtained from a single indentation test involving multiple unloading; therefore, the data points do not represent the average hardness values for any indentation depth. Average hardness values are shown in Fig. 6.

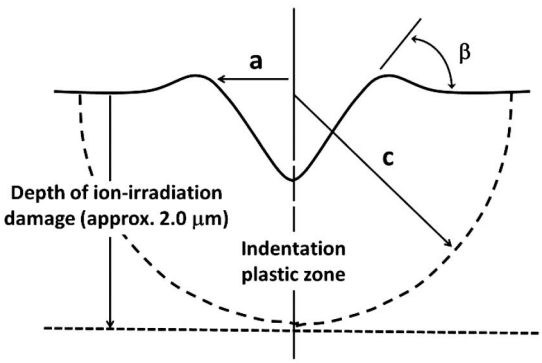

Fig. 5 Schematic illustration of an indentation and its associated hemispherical plastic zone of radius *c*. In our study, the indentations must be made at a small enough depth that *c* is less than the ion-irradiation depth.

as a function of annealing time, t, at 400°C. The hardness displays a logarithmic dependence upon annealing time. Curves of $H = H_{0\,\mathrm{dpa}} + At^n$ were fit to the data, and values of the parameters A and n were obtained for each dpa level. These equations for $H(t)$ were then used to determine the time t_c required for complete recovery of the irradiation damage, i.e., the annealing time needed for $H = H_{0\,\mathrm{dpa}}$.

Figure 8 depicts a logarithmic plot of t_c versus dpa for data obtained from tests performed primarily at annealing temperature of 400°C, followed by room-temperature indentation of 200 and 400 nm depth, on the AISI 310 and the Inconel 800H alloys. Linear regression analysis of the data indicates the following functional relationship between t_c (min) and irradiation damage (dpa)

$$t_c = 574(\mathrm{dpa})^{1.26} \tag{5}$$

The data suggest that the rate of thermal recovery of ion-induced crystallographic damage follows a single trend for both alloys and both indentation depths.

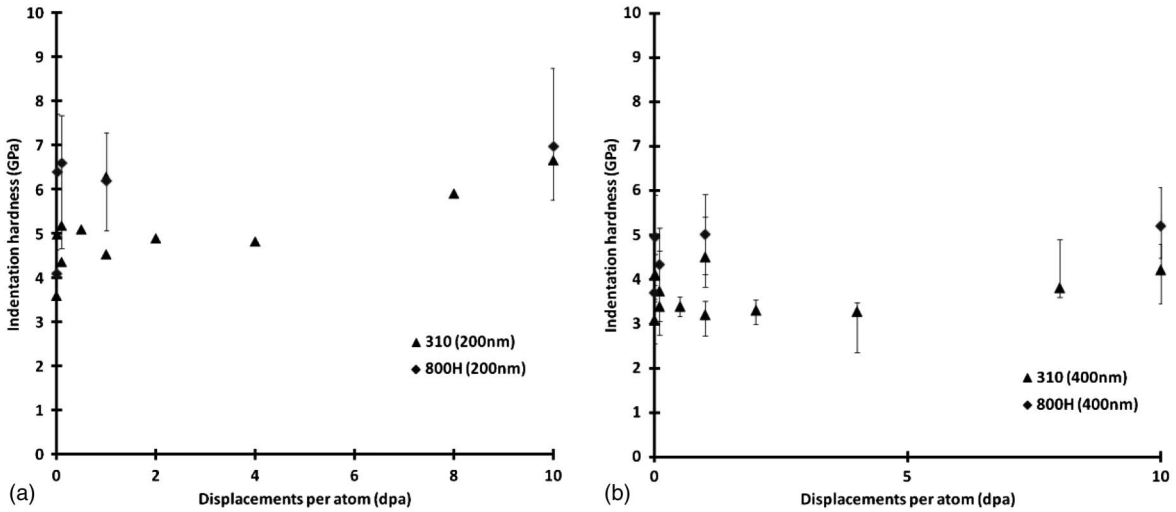

Fig. 6 Average indentation hardness versus Fe^{4+} ion irradiation damage for the AISI 310 and Inconel 800H alloys. The 200-nm deep indentations (*a*) show increased hardness compared to the 400-nm deep indentations (*b*) because of the indentation depth dependence of the hardness shown in Fig. 4 and discussed in Section 3.1.

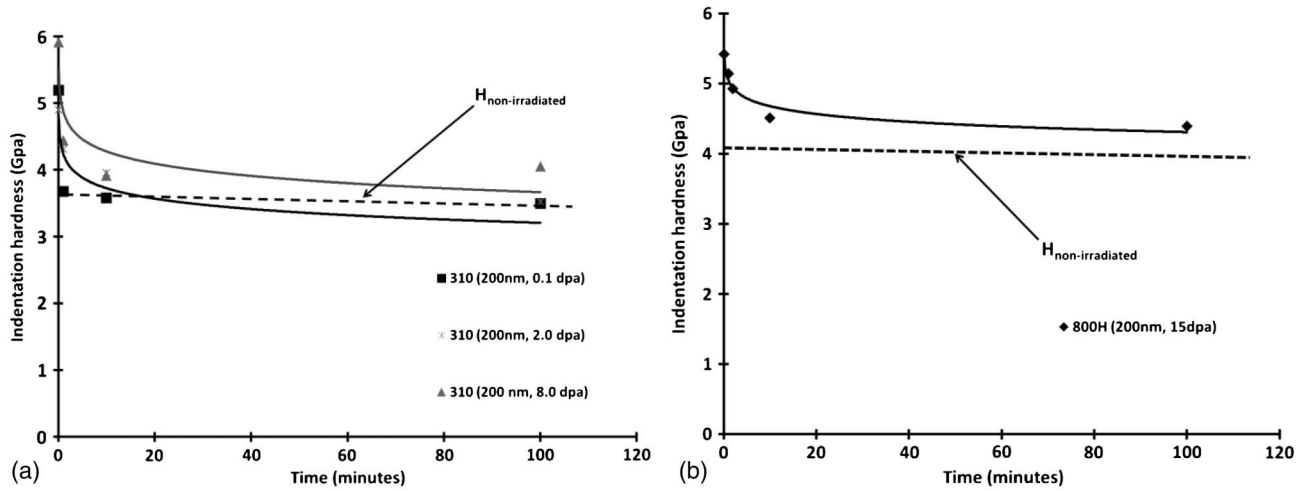

Fig. 7 Average indentation hardness, for indentation depth of 200 nm, versus 400°C annealing time for (*a*) AISI 310 and (*b*) Inconel 800H samples. The solid curves indicated power-law functions of time that were fitted to the data and were used to calculate the critical time t_c for complete recovery of the irradiation hardening.

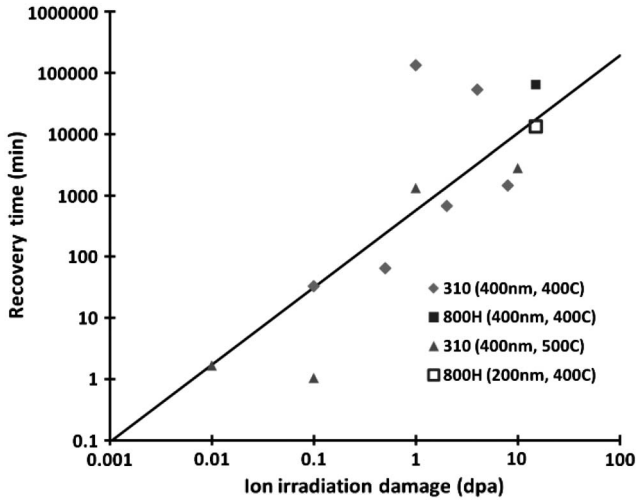

Fig. 8 Time t_c required to completely recover the irradiation hardness, by annealing at 400°C or 500°C, of the AISI 310 and Inconel 800H alloys versus dpa

Included in Fig. 8 are data from 400-nm depth hardness tests performed on the AISI 310 alloy at 500°C. These data lie on the same trend as the 400°C data, indicating that the rate of irradiation damage recovery is not significantly greater, within the precision limits of our measurement techniques, at 500°C than at 400°C.

The time for complete recovery of irradiation damage at 400°C and 500°C is quite short for these alloys. For example, Eq. (5) predicts that 1 dpa of irradiation damage, which is in the order of magnitude of the annual accumulated irradiation damage of in-core components, such as fuel cladding, is recovered in about 10 h at 400°C or 500°C.

It should be noted that we observed some oxidation on the surfaces of both alloys when annealed at 500°C, and this affected the 200-nm depth hardness measurements. The amount of oxidation was greater on the Inconel 800H than on the AISI 310 alloy, and in both materials, the heavily ion-irradiated regions displayed less oxidation than the nonirradiated regions. The effect of ion irradiation on the oxidation rate of these alloys is currently being investigated.

4 Conclusions

In this study, we performed Fe^{4+} ion irradiation, to damage levels up to 15 dpa, followed by isothermal annealing at 400°C and 500°C on samples of the AISI 310 and Inconel 800H alloys to assess (1) the dependence of indentation hardness upon ion-induced irradiation damage and (2) the rate of thermal recovery of the irradiation damage.

The average indentation hardness of both alloys increased very rapidly, by about 20–40%, with relatively small levels of ion irradiation corresponding to about 1 dpa. Our measured average hardness of the nonirradiated and the ion-irradiated material is similar, both in magnitude and dependence upon irradiation damage, to what was previously reported for similar alloys [15]. Similar power-law functions of $H(\text{dpa})$ were determined for both alloys, indicating that their hardness displayed similar dependence upon irradiation damage.

We observed that the ion-irradiation hardening in both alloys recovered rapidly with annealing at 400°C and 500°C. The time t_c for complete recovery of the irradiation damage was found to increase as a power-law function of dpa for both alloys at 400°C and for the AISI 310 alloy at 500°C.

Our findings suggest that in the case of high-temperature, in-core applications typical of those being proposed for fuel cladding and pressure tube liners in the Canadian Gen-IV SCWR concept, both AISI 310 and Inconel 800H alloys will undergo at least 20% increase in hardness as a result of low levels of neutron irradiation damage typical of what could be expected within 1 year in core. This increase will, however, be negated by very rapid concurrent thermal recovery. Our data suggest that the recovery rate is sufficiently rapid that no net irradiation hardening will occur. We are currently continuing our studies to more accurately quantify the rates of irradiation hardening and thermal recovery in these alloys.

An important other factor that will affect the actual rate of irradiation hardening and thermal recovery in these alloys is the rate of hardening resulting from accumulated hydrogen and helium transmutation products. We are currently expanding our study to implant samples of AISI 310 and Inconel 800H with various levels of helium to assess the resulting hardening and the rate at which the He-induced hardening recovers, if at all, with isothermal annealing.

In our study, we observed some oxidation on the surfaces of both alloys when annealed at 500°C. The amount of surface oxidation was greater on the Inconel 800H than on the AISI 310, and in both materials, the heavily ion-irradiated regions displayed less oxidation than the nonirradiated regions. This effect is currently being investigated further.

Acknowledgment

The technical assistance of Mr. Jack Hendriks at the Tandetron Ion Accelerator facilities at the University of Western Ontario (London, Ontario, Canada) is gratefully acknowledged. We wish to thank Ms. Maisaa Tawfeeq for providing the optical micrograph of the Inconel 800H alloy (Fig. 6). Finally, many helpful discussions concerning the findings of this study with members of the Canadian Gen-IV SCWR Materials Research Group, coordinated by Dr. David Guzonas, are also gratefully acknowledged.

The authors wish to acknowledge the financial support for this research from the Canadian federal government through a Collaborative Research and Development grant involving two departments: the Natural Science and Engineering Research Council (NSERC) and the Natural Resources Canada (NRCan).

Nomenclature

$A(h)$ = indentation area projected on a plane normal to the indentation direction, μm^2
c = radius of the indentation plastic zone, nm
dpa = displacements per atom
F = indentation force, mN
H = indentation hardness, GPa
h = indentation depth, nm
SCWR = supercritical water reactor
SRIM = stopping and range of ions in matter
t = annealing time, s
t_c = annealing time for complete recovery of irradiation hardening, s

Uncertainties

Ion irradiation dosage = $\pm 0.02\%$
Ion energy = $\pm 0.125\%$
Anneal temperature = ± 5°C
Indentation force, $F = \pm 0.4$ mN
Indentation depth, $h = \pm 0.4$ nm
Hardness = $\pm 5\%$

References

[1] Yetisir, M., Gaudet, M., and Rhodes, D., 2013, "Development and Integration of Canadian SCWR Concept With Counter-flow Fuel Assembly," Sixth International Symposium on Supercritical Water Reactors (ISSCWR-6), Shenzhen, Guangdon, China, Paper No. ISSCWR6-13059.
[2] U.S. DOE Nuclear Energy Research Advisory Committee; the Generation IV International Forum, 2002, "A Technology Roadmap for Generation IV Nuclear Energy Systems," The Generation IV International Forum (GIF-002-00).
[3] Bruemmer, S. M., Simonen, E. P., Scott, P. M., Andersen, P. L., Was, G. S., and Nelson, J. L., 1999, "Radiation-Induced Material Changes and Susceptibility to Intergranular Failure of Light-Water-Reactor Core Internals," J. Nucl. Mater., **274**(3), pp. 299–314.
[4] Dutton, R., and Lim, C. S., 1986, "Use of Accelerator Techniques to Study Irradiation Damage," Can. Metall. Q., **25**(2), pp. 169–180.
[5] Radjabov, T. D, 1991, "Modification of Physico-mechanical Properties of Metals and Metallic Coatings by Ion Implantation," Vacuum, **42**(1–2), pp. 163–168.
[6] Romanov, I. G., and Tsariova, I. N., 2003, "Influence of Low Dose Ion Irradiation on the Structure and Physical–Mechanical Properties of Solids," Vacuum, **68**(3), pp. 213–218.
[7] Li, N., Martin, M. S., Anderoglu, O., Misra, A., Shao, L., Wang, H., and Zhang, X., 2009, "He Ion Irradiation Damage in Al/Nb Multilayers," J. Appl. Phys., **105**(12), pp. 123522–123528.
[8] Hosemann, P., Dai, Y., Stergar, E., Leitner, H., Olivas, E., Nelson, A. T., and Maloy, S. A., 2011, "Large and Small Scale Materials Testing of HT-9 Irradiated in the STIP Irradiation Program," Exp. Mech., **51**(7), pp. 1095–1102.
[9] Doerner, M. F., and Nix, W. D., 1986, "A Method for Interpreting the Data From Depth-Sensing Indentation Instruments," J. Mater. Res., **1**(4), pp. 601–609.
[10] Nix, W. D., and Gao, H., 1998, "Indentation Size Effects in Crystalline Materials: A Law for Strain Gradient Plasticity," J. Mech. Phys. Solids, **46**(3), pp. 411–425.
[11] Johnson, K. L., 1985, "Normal Contact of Inelastic Solids," *Contact Mechanics*, K. L. Johnson, ed., Cambridge University Press, Cambridge, pp. 153–184.
[12] Tabor, D., 1951, "Deformation of Metals by Spherical Indenters," *The Hardness of Metals*, D. Tabor, ed., Clarendon Press, Oxford, pp. 44–83.
[13] Murakami, Y., and Itokazu, M., 1997, "Elastic-plastic Analysis of a Triangular Pyramidal Indentation," Int. J. Solids Struct., **34**(30), pp. 4005–4018.
[14] Larsson, P.-L., Giannakopoulos, A. E., SÖderlund, E., Rowcliffe, D. J., and Vestergaard, R., 1996, "Analysis of Berkovich Indentation," Int. J. Solids Struct., **33**(2), pp. 221–248.
[15] Hunn, J. D., Lee, E. H., Byun, T. S., and Mansur, L. K., 2000, "Helium and Hydrogen Induced Hardening in 316LN Stainless Steel," J. Nucl. Mater., **282**(2–3), pp. 131–136.